NATURAL VENTILATION IN A ROOM, TRANSITION FROM NATURAL TO ADVERSE FORCED CONVECTION

Sébastien Wullens[1,2], Michel Pons[2], Étienne Wurtz[3], Yann Fraigneau[2]
[1] LOCIE - CNRS UMR5271, Université de Savoie, Le Bourget du Lac, France
[2]LIMSI - CNRS UPR3251, Orsay, France
[3]CEA - INES, Le Bourget du Lac, France

ABSTRACT

This study presents 2D numerical simulations of natural ventilation in a room equipped with two openings, one low and one high. The main features are commented in terms of flow and heat transfer. We first focus on pure natural convection within the framework of the ADNBati benchmark, and validate the numerical model this way. Then we study the transition to adverse forced convection (the flow is eventually reversed) and highlight the main changes due to transition. Lastly, we present a method for coupling CFD simulations with a multizone model.

INTRODUCTION

The purpose of reducing global energy consumption makes it necessary to avoid, or at least limit, the use of air conditioning systems during hot periods. Natural ventilation is one way to refresh buildings with low energy consumption. For building designers to guarantee the performance of this technique, they must have tools for accurately computing the rate of heat transfer in given conditions. The most reliable tools currently used for simulating ventilation in a whole building are multizone models (Stephan, 2010; Chen et al., 2010). These models are quite reliable for predicting wind-induced flows (forced convection) in buildings. However, the assumptions they rely on, e.g. pressure and temperature homogeneity in each zone, have not been verified in cases when convection is only *natural*, i.e. strictly thermally-induced, or mixed (Axley, 2007). As a result, multizone simulations may substantially differ from reality and from detailed Navier-Stokes simulations, even in very simple cases (Mora et al., 2003; Pons et al., 2012). One significant current research trend consists of feeding multizone models with new correlations, the validation of which requires considerable experimental equipment (Chen et al., 2010). Computational fluid dynamics (CFD), i.e. a direct numerical solution to Navier-Stokes equations, may limit the need for such heavy experimental tests as long as the purpose is to establish reduced order models or parametric correlations. CFD simulations of whole buildings are out of reach, however, unless CFD is coupled to multizone models, for instance in an interoperability platform. According to Wang and Wong (2009) this coupling is optimal when the pressure-based boundary conditions are imposed on the CFD code.

Although pressure-based boundary conditions are often used in building simulations (Axley, 2007; Chen et al., 2010), they are rare in CFD where conditions on velocity are much more common. We have therefore implemented pressure-based boundary conditions at openings into an in-house CFD code; this article presents our preliminary results. The first part present pure natural convection; the results are compared to those of Brangeon et al. (2011) obtained in the PIMENT laboratory. The second part discusses mixed convection for low Reynolds numbers.

MODEL DESCRIPTION

Test case geometry, heat and fluid flow equations

The geometry is described in the ADNBati benchmark (Pons et al., 2012). It is a two-dimensional model of one room of the Charpak building in the IESC, Cargèse, France (see Figs. 1 and 2).

Figure 1 The Charpak building

The length of the cavity is $L = 6.50m$ and its height is $H = 2.50m$. It is equipped with two openings on opposite sides provided with dampers. The inside wall temperature is assumed to be invariable in space and time at $T_p > T_o$. This assumption cancels the effects of conduction within walls and radiative transfers between them. In this study, due to low temperature gaps between the walls and surrounding air, the flow is laminar and the Boussinesq approximation is verified.

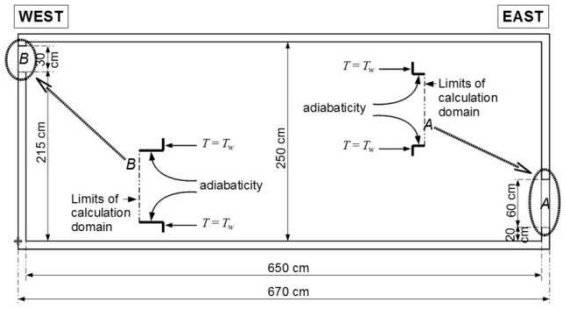

Figure 2 The geometry of the room

The mass, momentum and heat equations, written in dimensionless form, are written as follows:

$$\nabla \mathbf{u} = 0 \tag{1}$$

$$\frac{\partial \mathbf{u}}{\partial t} + \nabla.(\mathbf{u} \otimes \mathbf{u}) = -\nabla p + \frac{1}{Re}\nabla^2 \mathbf{u} + \theta Ri \mathbf{e_z} \tag{2}$$

$$\frac{\partial \theta}{\partial t} + \nabla.(\mathbf{u}\theta) = \frac{1}{RePr}\nabla^2 \theta \tag{3}$$

with $\mathbf{u}$ the velocity vector, $p = \Pi + z/Fr$ the deviation of the dynamic pressure from the hydrostatic pressure and $\theta = (T\text{-}T_o)/(T_p\text{-}T_o)$ the temperature, where T_o=25°C is the temperature of the surroundings. Thermo-physical properties α, ν, c_p and β are assumed invariable in space and time and given at this temperature. The velocity, length, and pressure are scaled by u_o, H and ρu_o^2, with :

$$u_0 = \sqrt{(P_B - P_A)/\rho} + (\alpha / H)\sqrt{Ra} \tag{4}$$

$$Ra = g\beta(T_p - T_o)H^3 / \nu\alpha \tag{5}$$

The parameters leading the flow are the Richardson, the Reynolds and the Prandtl numbers, written as:

$$Ri = g\beta(T_p - T_o)H / u_o^2 \tag{6}$$

$$Re = u_o H / \nu \tag{7}$$

$$Pr = \nu / \alpha \tag{8}$$

In the case of pure natural convection, $(P_B\text{-}P_A) = 0$. Therefore, the parameters become:

$$1/Re = Pr\sqrt{Ra} \tag{9}$$

$$Ri = Pr \tag{10}$$

Thus, traditional dimensionless numbers of pure natural convection flows appear (Brangeon et al., 2011).

Boundary conditions

Temperature is assumed invariable in space and time on the walls, θ_p=1. There is an exception for frame dampers, which are assumed adiabatic, $\nabla\theta.\mathbf{n} = 0$ (cf. Fig. 2). The air entering the domain is assumed to be at the temperature of the surroundings, θ_O=0. The air outlet is assumed to be adiabatic.

A non-slip boundary condition is applied to the walls for velocity and pressure. The choice of the conditions on the openings is a delicate point, still discussed in the fluid mechanics literature (Desrayaud et al., 2007). Here, the normal velocity gradient is set to zero, $\nabla(\mathbf{u}.\mathbf{n}).\mathbf{n} = 0$. To ensure that the velocity divergence is null, the tangential velocity is also set to zero, $\mathbf{u}.\boldsymbol{\tau}$=0. Two different sets of pressure boundary conditions have been studied bellow. The first one is used to compare our results with the ADNBati benchmark:

- On opening A, if $\mathbf{u}.\mathbf{n}_A < 0$, then

$$p = -(0.5 / A_A) \times \int_{A_{inA}} (\mathbf{u}.\mathbf{n}_A)^2 dA \tag{11}$$

- On opening B, if $\mathbf{u}.\mathbf{n}_B \geq 0$, then p=0, else

$$p = -0.5 \times (\mathbf{u}.\mathbf{n}_B)^2 \tag{12}$$

The condition on the B opening is slightly different from the ADNBati benchmark to ensure the pressure continuity when a recirculation cell appears (e. g. Brangeon et al., 2011). For mixed convection study, equation (12) is applied to the two openings. An additional term takes into account the pressure gradient between the two openings:

- If $\mathbf{u}.\mathbf{n}_Z \geq 0$, then

$$p = -0.5\left(\left(1 - \sqrt{\frac{Ri}{Pr}}\right)^2 .\mathbf{n}_Z.\mathbf{e_x}\right) \tag{13}$$

- else,

$$p = -0.5\left(\left(1 - \sqrt{\frac{Ri}{Pr}}\right)^2 .\mathbf{n}_Z.\mathbf{e_x} + (\mathbf{u}.\mathbf{n}_Z)^2\right) . \tag{14}$$

Solving method

These conditions were implemented on a pre-existing finite volume code. It uses a standard incremental pressure-correction scheme with a second order Euler time splitting (Guermond et al, 2006). The non-linear term of the Navier-Stokes equation is extrapolated forward in time using the Adams-Bashford method. The prediction step is solved using ADI decomposition and the projection step is solved using a multigrid method coupled with a Gauss-Seidel algorithm. The volume is meshed using a rectilinear staggered grid.

To make the implementation of the new boundary conditions easier, their resolution is explicit in time.

Monitored variables

Common average quantities on walls and openings are compared in this study. The analysis concerns:

- The net flow rates entering the openings (with Z=A or B)

$$q_{inZ} = \int_{A_Z} \frac{|\mathbf{u}.\mathbf{n}_Z| - \mathbf{u}.\mathbf{n}_Z}{2} dA \tag{15}$$

- The global flow rate

$$q_v = -\int_{A_A} \mathbf{u}.\mathbf{n}_A \, dA = \int_{A_B} \mathbf{u}.\mathbf{n}_B \, dA \qquad (16)$$

- The Nusselt numbers on each wall j (with j=w, *e*, *c* or *f*, respectively, for *west, east, ceiling* and *floor*)

$$Nu_j = \frac{1}{A_j} \int_{Aj} (\nabla\theta \mathbf{n}_j).dA \qquad (17)$$

- The average temperature of the outgoing flow (with Z=A or B)

$$\bar{\theta}_Z = \frac{\left(\int_{A_Z} \frac{|\mathbf{u}.\mathbf{n}| + \mathbf{u}.\mathbf{n}}{2} \theta.dA \right)}{\left(\int_{A_Z} \frac{|\mathbf{u}.\mathbf{n}| + \mathbf{u}.\mathbf{n}}{2} .dA \right)} \qquad (18)$$

- The global flow rate (in $m^3.h^{-1}$)

$$Q_v = 3600 H^2 u_0 q_v \qquad (19)$$

- The cooling rate (in W)

$$Q_h = \rho c_p \left(T_p - T_o\right) H^2 u_0 \sum_{Z=A,B} [(q_v - q_{in\,Z})\bar{\theta}_Z] \qquad (20)$$

PURE NATURAL CONVECTION

For simulating thermo-convective flows, equations (11) and (12) are used as boundary conditions. Our results are then validated by comparison with an independent previous simulation of the same problem (Brangeon et al., 2011, hereafter abbreviated as *B&al*). Various features related to ventilation and heat-transfer characteristics are highlighted.

Global data

In addition to the cross-ventilation flow-rate Q_v and the total cooling rate Q_h defined above, we will also consider the contribution of each wall to the total cooling rate and the average outlet temperature $\bar{\theta}_B$. The values are given in Table 1. Our results agree very well with those of *B&al*: whatever data are considered deviation is less than 1% for $Ra=10^5$ and always remains under 4%, even if it seems to grow with the Rayleigh number. The influence of the details of the numerical scheme on the results is weak. Velocity in boundary layers induced by natural convection is usually expected to scale in $Ra^{0.5}$; we instead obtain a scale law in $Ra^{0.44}$ for the total flow-rate, a feature that will be explained when considering the flow pattern. The Nusselt numbers on (i) the eastern wall and on the floor scale, (ii) the ceiling, and (iii) the western wall, respectively practically scale in (i) $Ra^{0.34}$, (ii) $Ra^{0.28}$, and (iii) $Ra^{0.4}$-$Ra^{0.6}$, which is representative of heat transfer in, respectively (i) the turbulent regime, (ii) the laminar regime, and (iii) heat-transfer intensification by a jet-effect. Considering the size of each wall (see Fig. 2), the respective contributions to the total heat-transfer can be evaluated when *Ra* changes from 10^5 to 10^7. The contributions of the eastern wall and the ceiling do not change much, resp. 20 and 10%. The contributions of the floor and of western wall change significantly, from 60+10% to 50+20%. The study of the flow pattern shows that this change is related to the occurrence of a jet-like average flow inside the room. As a result, the air stream crosses the room faster and faster when the *Ra* number increases and has less and less time for heating up, so that the non-dimensional temperature of the fluid leaving the room, $\bar{\theta}_B$, significantly decreases.

Flow patterns

Figures 3 and 4 show the average flow patterns, respectively for $Ra=10^5$ (steady laminar flow) and $Ra=10^7$ (unsteady flow with low turbulence). Again, our results agree very well with those of *B&al*. Generally speaking, the flow enters the room through the lower opening (opening A on the eastern wall), produces a crawling jet stuck on the floor and climbs along the western wall before leaving the room by the high opening (opening B on the western wall). A secondary flow makes a vertical boundary layer along the eastern wall and feeds a slow warm horizontal boundary layer just beneath the ceiling. Thirdly, two recirculation cells occupy a large part of the volume at the center of the room. Between the two cells, the flow is unexpectedly re-directed toward the inlet opening A. We call this feature the *return flow*.

The increase in Rayleigh number makes all the boundary layers thinner; it also makes the main flow (crawling jet) thinner and faster. As a result, the two recirculation cells grow and occupy the major part of the room.

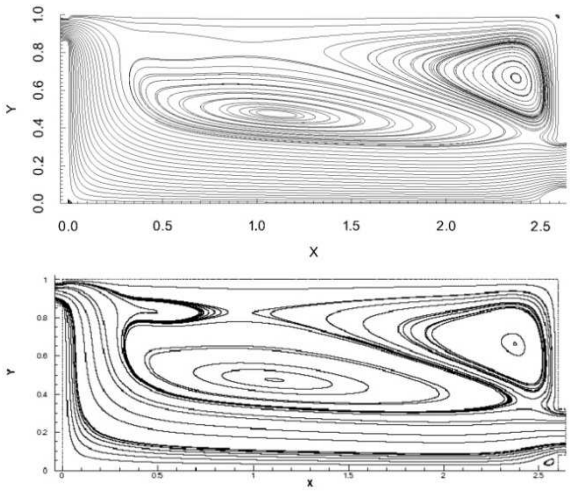

Figure 3 Streamlines for $Ra=10^5$ (case H), our results (top) compared to those of B&al (bottom). Opening A on the right, opening B on the left.

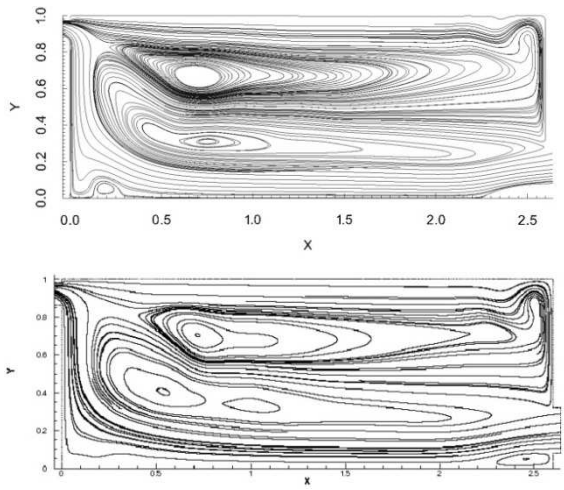

Figure 4 Streamlines for Ra=10^7 (test J), our results (above) compared to those of B&al (under).

The latter feature does not favour thermally-induced natural ventilation, neither in terms of air renewal nor cooling efficiency. This point deserves further investigation, e.g. on the means for enhancing air mixing within the room.

Velocity profiles at the openings

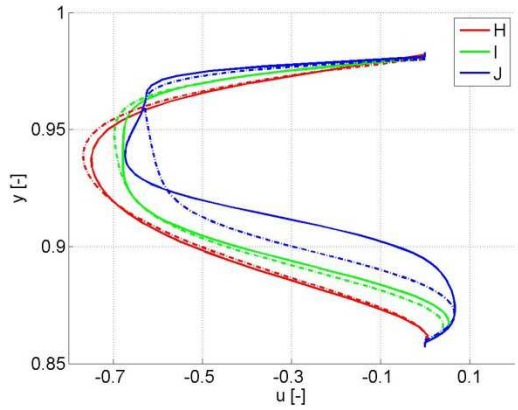

Figure 5 Profiles of horizontal velocity at opening B, cases H J (cf. Table 1). Results of B&al in dashes.

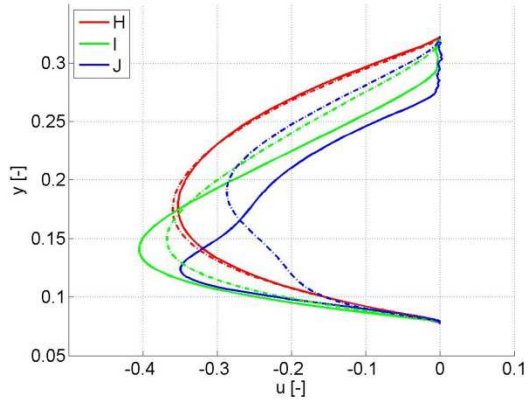

Figure 6 Profiles of horizontal velocity at opening A, cases H J (cf. Table 1). Results of B&al in dashes.

Figures 5 and 6 show the profiles of horizontal velocity at openings B and A for the three values of *Ra*. Our results agree well with those of *B&al* at a low Rayleigh number. However, for *Ra*=10^7 significant differences appear, which are surely due to differences in the discrete implementation of the boundary conditions. These differences are the cause of the deviations previously observed on global data.

The profiles exhibit two main features. First, for *Ra*≥10^6 some air enters at the bottom of opening B. This small recirculation cell is created by the strong bending of the stream between the vertical boundary layer along the western wall and the exit flow which is horizontal. This small cell partly blocks the exit of the main flow; this blocking explains why the global flow-rate scales in $Ra^{0.44}$ instead of $Ra^{0.50}$. Second, for *Ra*=10^7 part of the inlet velocity profile at the opening A almost vanishes. Indeed, with an intense enough convection, the *return flow* (between the two main recirculation cells) is strong enough for partly blocking the inlet flow.

This analysis shows that cooling by ventilation induced by natural convection only might be less efficient than expected and still deserves attention.

MIXED CONVECTION

Description of the test cases

First, equations (13) and (14) are used as boundary conditions. The influence of these boundary conditions can be evaluated by comparing cases H (natural convection) and A (mixed convection), designed with almost the same Richardson number but with either boundary condition. The results are similar. This shows again that, in the present configuration, the flow is not very sensitive to the details of the boundary conditions.

In the following, the Rayleigh number is fixed at *Ra*=10^5, except for case G where *Ra*=0. The Richardson number is changed from *Ri*=*Pr* (pure natural convection) to *Ri*=0 (pure forced convection). This change corresponds to an increase of the total pressure difference (e.g. induced by wind) between the two openings while keeping the wall temperature constant (except for case G). It is obviously more useful to study adversity between forced convection and natural convection. Case G is isothermal and designed with the same pressure difference between openings as in case F.

Here again we analyse the global data, the flow patterns and the velocity profiles at the openings.

Global data

In cases E and F, the flow is globally reversed compared to case A. Reversal takes place between cases D and E. In case E, some air leaves the room at opening A simply because of a small recirculation cell there. Reversal would deserve a specific study, but we are focusing herein on the effects of reversal on the cooling rate and the flow pattern. Table 3

gives the global data related to heat-transfer. From case A to D, ventilation tends to decrease due to a stronger and stronger forced resistance to thermo-convection. Both the global flow-rate and global cooling rate decrease. Due to the same effect as described above, the mean outlet temperature $\overline{\theta}_B$ increases. It can also be seen that the distribution of heat-transfer between the four walls is not substantially modified, a feature that can surely be related to the relative stability of the flow pattern from case A to case D.

Beyond flow reversal (cases E and F), cooling distributes completely differently between the four walls. The Nusselt number at the ceiling becomes larger than the other ones, with a noticeable decrease on the floor and eastern wall. This trend can be easily explained with the flow patterns.

Flow patterns

Figures 7 10 show the flow patterns of cases A, and D G. All these cases are stationary.

Even when the adverse pressure difference is not large enough to reverse the flow direction, it reduces both the global flow-rate and the extracted heat-rate similarly (almost a factor of 2 from case A to case D). However, there is a significant change in the flow pattern and in the contributions of each wall to the total heat transfer. Because of the adverse pressure gradient, the two recirculation cells in the centre of the room grow and eliminate the two boundary layers along the eastern wall and just underneath the ceiling, see Fig. 7. Thus, the heat fluxes at these two walls drop significantly. In addition, the air in the floor boundary layer flows slowly, it heats up almost completely so that the heat flux at the western wall also drops significantly. As a result, 69% of the total heat extracted comes from the floor alone. This result demonstrates that the heat flux can be very unevenly distributed between the different walls of a room.

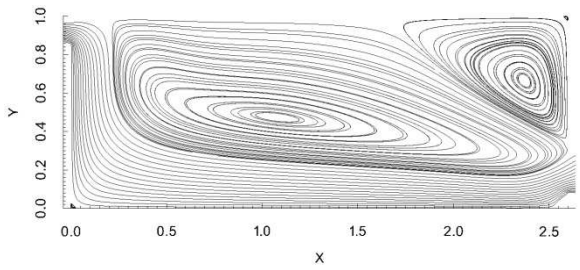

Figure 7 Flow pattern with Ra=10^5 and Ri=0.292 (case D see Table 2)

When the adverse pressure gradient is strong enough, the air flow is reversed and the flow pattern changes dramatically. Now cold air enters the room by the high opening B and forms a jet that first sticks to the ceiling because of the well-known Koanda effect (see Figs. 8 10). Eventually, this cold jet falls by flowing between the two recirculation cells thus separating them and it finally leaves the room by the low opening A. The completely modified flow pattern now makes the ceiling exchange a significant heat-rate (40% of the total), while each the two vertical walls only transfers a small amount (10 11% of the total) because they are only in contact with recirculation cells. It can also be seen that the heat flux exchanged by the floor strongly depends on the distance after which the jet falls.

The only change from case F to case G is that the latter is isothermal (walls and outdoor air are at the same temperature). Figure 10 shows how much the flow pattern is changed: the low and western recirculation cell grows very much while the high and eastern one shrinks, probably due to the pressure exerted by the incoming jet.

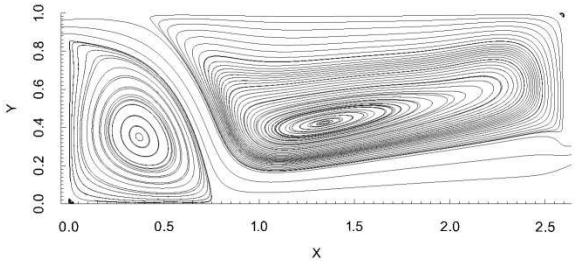

Figure 8 Flow pattern with Ra=10^5 and Ri=0.223 (case E, see Table 2)

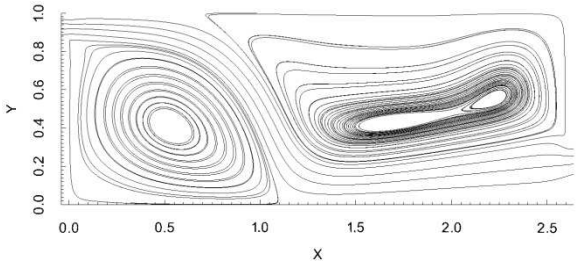

Figure 9 Flow pattern with Ra=10^5 and Ri=0.188 (case F, see Table 2)

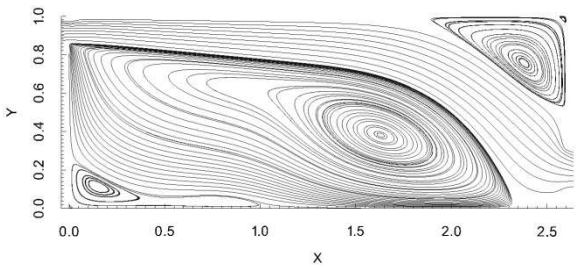

Figure 10 Flow pattern with Ra=0 and Ri=0 (case G)

Velocity profiles at the openings

Among all the results of our numerical simulations, the velocity profiles at the openings surely are the most sensitive to the boundary conditions. Figures 11 and 12 display the horizontal velocity profiles at openings A and B, respectively, for all the cases described in Table 2.

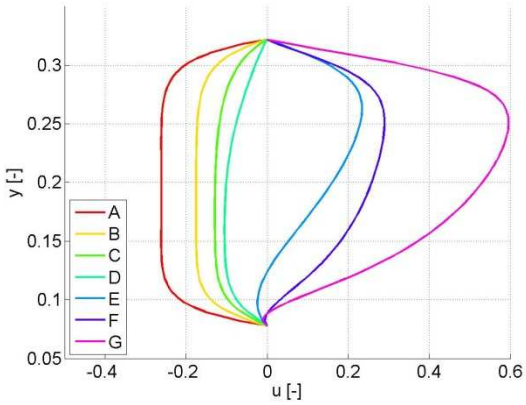

Figure 11 Profiles of the horizontal velocity at opening A. Cases A G.

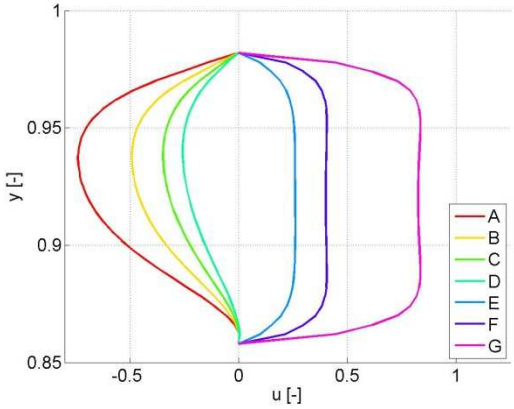

Figure 12 Profiles of the horizontal velocity at opening B. Cases A to G.

The profiles of case A are to be compared to those of case H in Figures 5 and 6. The former profiles are almost those of a plug flow (therefore not yet established), whereas the latter ones are almost parabolic (established flow). Desrayaud et al. (2007) described similar differences, raising the issue of likelihood. A partial experimental proof was given by Chérif et al. (2010). These authors measured the fluid velocity profile at the inlet of a vertical chimney: the experimental profile is closer to the flat one (case A) than to the parabolic one (case H).

Our calculations show that, when the cavity is much wider than the openings, the details of the inlet and outlet profiles only have a weak influence on global data such as the flow rate crossing the room and total rate of extracted heat. Even the distribution of the heat-rate between the four walls is practically unchanged.

PERSPECTIVES

The Rayleigh numbers studied herein are relatively low. The next step to approach building behaviour will be to increase these numbers. Correlations such as q_v =f(*Ri*,*Re*) and *Nu*=f(*Ri*,*Re*) are expected from the results of this computation.

A first way to use this work would be to implement these correlations as a "*box*" in a multizone model of a whole building based on the "*Buildings*" library in "*Modelica"* (Wetter et al., 2011). However, since the correlations are obtained after averaging the results of the steady state over time, this simple way of using the results is valid only if the transient state has no influence on the building's behaviour.

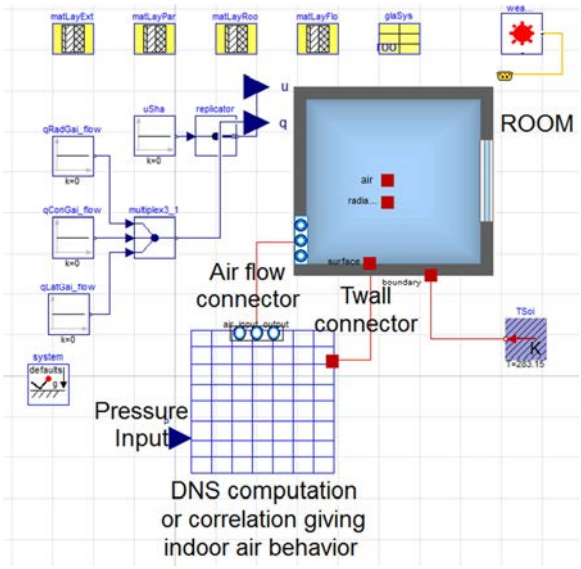

Figure 13 Development of a coupling method with the Modelica package "Buildings"

A second way to use CFD results would be to combine this calculation in time with the multizone simulation. Knowing wall temperatures from the multizone model and pressure differences from adapted weather data, the CFD computation could give flow values and Nusselt numbers to the multizone simulation in return. This kind of coupling would consider transient state and steady state because all the computation would be averaged over time on the multizone time step. This kind of coupling would cost a great deal of computation time. Several strategies are explored in the literature to lower these costs such as changing the coupling variables, choosing adapted coupling time steps or of course using other methods than a direct Navier-Stokes computation.

Lastly, even if in this study the change of the Bernoulli boundary condition seems to have a limited effect on the flow-rate and the rate of heat extracted, this statement still needs to be validated for higher Rayleigh numbers.

CONCLUSION

The present CFD results for the ADNbati benchmark confirm previous ones obtained with a different numerical method. Work should be continued, first to better understand the effects of the detailed boundary conditions, then to extend the scale laws ($Ra^{0.44}$ for the total flow-rate) and the magnitude of heat

extraction to the range of Rayleigh numbers found in real buildings.

Finally, the study of mixed convection highlights the changes of the distribution of heat extraction from the walls. The Nusselt number at the ceiling becomes larger than the others, with a noticeable decrease on the floor and eastern wall when the adverse forced flow is predominant. This trend can be explained with the flow patterns.

NOMENCLATURE

A	surface, m^2
cp	thermal capacity, $J.kg^{-1}.K^{-1}$
g	standard gravity, $m.s^{-2}$
H	room height, m
L	room length, m
n	normal vector, -
p	pressure, -
Pr	Prandtl number, -
q_{inZ}	flow rate entering through opening Z
q_v	global flow rate, -
Qv	global flow rate, $m^3.h^{-1}$
Qh	cooling rate, W
Ra	Rayleigh number, -
Re	Reynolds number, -
Ri	Richardson number, -
Nu_p	Nusselt number (wall p), -
t	time, -
T	temperature, K
u	velocity vector, -
(x,z)	spatial coordinates, -
Greek symbols	
Π	static pressure, -
β	thermal expansion coefficient, K^{-1}
α	thermal diffusivity, $m^2.s^{-1}$
ν	kinematic viscosity, $m^2.s^{-1}$
θ	temperature, -
ρ	density, $kg.m^{-3}$
Subscripts and superscript	
A, B	related to opening A or B
i	related to indoor air
o	related to outdoor air
ref	reference
p	related to walls
w,e,f,c	respectively for *west, east, floor* and *ceiling*

ACKNOWLEDGEMENT

This work was supported by the French *Agence Nationale de la Recherche* and its *Habitat intelligent et solaire photovoltaïque programme* (4C project n°ANR-08-HABISOL-019).

REFERENCES

Axley J., 2007. Multizone airflow modeling in buildings: history and theory. HVAC&R Research. Vol. 13(No. 6): pp. 907-928.

Brangeon B., Bastide A., Joubert P. et Pons M., 2011. Étude numérique de la ventilation traversante naturelle dans une cavité ouverte. Application au rafraîchissement passif des locaux, Congrès Français de Thermique, ISBN 978-2-905267-76-4, No 177.pdf: pp. 213-218.

Chérif Y., Joulin A., Zalewski L., Lassue S., 2010. Outils pour l'étude expérimentale de la convection naturelle entre plaques planes verticales différentiellement chauffées, proc. of the annual Congrès Français de Thermique, Vol. 18.

Desrayaud G., Bennacer R., Caltagirone J.-P., Chenier E., Joulin A., Laaroussi N. and Mojtabi K., 2007. Etude numérique comparative des écoulements thermoconvectifs dans un canal vertical chauffé asymétriquement, VIIIème Colloque Inter-Universitaire Franco-Québécois (Montréal, Canada, 28-30 May, 2007), CIFQ2007/ART-2006-2014.

Guermond JL., Minev P., and Shen J., 2006. An overview of projection methods for incompressible flows. Computer methods in applied mechanics and engineering, Vol. 195: pp. 6011-6045.

Mora L., Gadgil A.J., Wurtz E., 2003. Comparing zonal and CFD model predictions of isothermal airflows to experimental data, Indoor Air Journal Vol. 13: pp. 77-85.

Pons M. et al., 2012. Le cas-test ADNBATI, un benchmark sur la ventilation naturelle dans une pièce d'habitation, Congrès Français de Thermique, ISSN 1259-164X, Vol. 1 pp. 262-269.

Stephan L., 2010. Modélisation de la ventilation naturelle pour l'optimisation du rafraîchissement passif de bâtiments, Thèse Université de Savoie, Le Bourget-du-Lac.

Wang L. and Wong NH., 2009. Coupled simulations for naturally ventilated rooms between building simulation (BS) and computational fluid dynamics (CFD) for better prediction of indoor thermal environment, Building and Environment, Vol.44: pp. 95-112.

Wetter M., Zuo W., Nouidui TS., 2011. Modeling of heat transfer in rooms in the modelica "Buildings" Library, Proc. of Building Simulation 2011: 12-th Conference of International Building Performance Simulation Association, Sydney, 14-16 November.

Table 1

Comparison of natural convection results computed for this study with those of Brangeon et al. (reported in italic) for different Rayleigh numbers

Case	Ra	q_v	Nu_w	Nu_c	Nu_e	Nu_f	$\overline{\theta}_B$	Q_v	Q_h
		-	-	-	-	-	-	$m^3.h^{-1}$	W
H	10^5	0.0230 *0.0230*	1.56 *1.58*	0.79 *0.80*	3.32 *3.41*	3.61 *3.61*	0.86 *0.85*	1.47 *1.47*	2.95×10^{-5} *2.96×10^{-5}*
I	10^6	0.0207 *0.0209*	6.90 *7.21*	1.48 *1.49*	7.74 *7.49*	8.01 *8.01*	0.71 *0.70*	4.19 *4.23*	6.89×10^{-4} *6.85×10^{-4}*
J	10^7	0.0173 *0.0180*	17.83 *17.41*	2.89 *2.97*	17.15 *17.60*	17.08 *17.95*	0.58 *0.55*	11.08 *11.43*	0.0150 *0.0155*

Table 2

Mixed convection for $Ra=10^5$ (except for case G where Ra=0) and various Richardson numbers, global data: q_{inX} non-dimensional net inlet flow-rate at opening X (X=A or B), q_v non-dimensional cross-ventilation flow-rate and Q_v dimensional cross-ventilation flow-rate.

Case	Ri	Re	q_{inA}	q_{inB}	q_v	Q_v
	-	-	$\times10^{-2}$	$\times10^{-2}$	$\times10^{-2}$	$m^3.h^{-1}$
A	0.711	445	2.26	0	2.26	1.45
B	0.413	584	1.49	0	1.49	1.25
C	0.329	655	1.03	0	1.03	0.973
D	0.292	694	0.745	0	0.745	0.744
E	0.223	795	0.02	1.12	-1.12	-1.28
F	0.188	865	0	1.82	-1.82	-2.27
G	0	420	0	5.11	-5.11	-3.09

Table 3

Thermal average values of mixed convection computation for $Ra=10^5$ and various Richardson numbers

Case	$\overline{\theta}_A$	$\overline{\theta}_B$	Nu_w	Nu_c	Nu_e	Nu_f	Q_h
	-	-	-	-	-	-	$W\times10^{-5}$
A	-	0.865	1.51	0.771	3.32	3.55	2.92
B	-	0.89	1.19	0.62	2.83	3.3	2.59
C	-	0.92	0.767	0.424	2.09	2.84	2.08
D	-	0.921	0.497	0.282	1.5	2.38	1.59
E	0.837	-	0.869	1.67	0.493	0.09	2.54
F	0.786	-	2.5	3.52	2.4	3.3	4.16